Available online at www.sciencedirect.com
ScienceDirect
Journal of Non-Crystalline Solids 353 (2007) 4792–4800
JOURNAL OF NON-CRYSTALLINE SOLIDS
www.elsevier.com/locate/jnoncrysol

The local environment of trivalent lanthanide ions in sodium silicate glasses: A neutron diffraction study using isotopic substitution

Martin Wilding [a,*,1], Yaspal Badyal [b,2], Alexandra Navrotsky [a]

[a] Thermochemistry facility, University of California at Davis, Davis, CA 95616, United States
[b] Intense Pulsed Neutron Source, Argonne National Laboratory, 9700 S. Cass Avenue, Argonne IL 60439, United States

Received 4 October 2006
Available online 22 August 2007

Abstract

Neutron diffraction data on lanthanide-bearing sodium silicate glasses were collected using the glass, liquid and amorphous materials diffractometer (GLAD) at the intense pulsed neutron source (IPNS), Argonne. Measurements were made on four glass samples; a sodium silicate base glass with no added lanthanide, a sample with 6 mol% La_2O_3 added to the base composition, and two isotopically-distinct samples containing 6 mol% Dy_2O_3. Of the Dy-bearing samples, one contained natural enrichment Dy, and the other a 'null scattering' mixture of natural and ^{162}Dy isotopes. The first-order isotope difference of the scattering from the Dy-bearing samples revealed a Dy–O nearest-neighbor distance of 2.3 Å and a mean coordination number of 5.9 oxygen atoms around each dysprosium ion; the latter is in good agreement with the coordination number derived from bond–valence theory. The results for the La-bearing glass were also consistent with a sixfold coordination of oxygen atoms around the rare earth. The diffraction data are used in combination with Reverse Monte Carlo modeling techniques to interpreter the structural role of the rare earth ions. From these models, it is apparent that there is competition between monovalent sodium ions and the rare earth ions for the same non-bridging oxygen atoms. As a result the addition of rare earth ions appears to cause disruption of the Na-rich percolation domains characteristic of the sodium silicate base glass. These neutron results are consistent with the formation of a specific lanthanide Q^3 as suggested by NMR and Raman spectroscopy, but offer no direct evidence for the formation of 'oxide-like' lanthanide clusters.

Keywords: Neutron diffraction/scattering; Monte Carlo simulations; Silicates; Rare-earths in glasses; Medium-range order; Short-range order

1. Introduction

Composition, and hence structure, has a big impact on the solubility of rare earth (RE) ions in silicate liquids and glasses [1,2]. The luminescence properties closely coupled the dispersion of RE ions throughout the glass network because the fluorescence is strongly influenced by the local environment [3,4]. The RE local structure also affects the physical properties of RE-bearing glasses, for example, the potential for leaching and the long-term stability of the glass host. Along with the potential for clustering, which impacts the effectiveness of neutron-absorbing ions such as Gd(III), these are crucial considerations in the evaluation of proposed radioactive waste hosts [3,5].

The behavior of RE ions in silicate liquids is also of interest to the geochemical community. In particular, the concentrations of these elements are used as indicators for both the origin and evolution of magmatic systems [6]. Although the partitioning of RE ions between liquids and crystallizing phases is frequently described in terms of liquid structure [7], little is understood about the activity of RE components in natural silicate liquids.

The lanthanide series has a high formal charge so it is not surprising that RE ions have a strong influence on glass

* Corresponding author.
[1] Present address: Institute of Mathematical and Physical Sciences, The University of Wales, Aberystwyth, Aberystwyth, Ceredigion SY23 3BZ, UK.
[2] Present address: Chemical Sciences Division, Oak Ridge National, Laboratory, Oak Ridge, TN 37831-6110, United States.

0022-3093/$ - see front matter © 2007 Elsevier B.V. All rights reserved.
doi:10.1016/j.jnoncrysol.2007.06.071

and liquid structure [8,9]. Neutron diffraction has proved to be particularly valuable tool for the study of such problems involving glass and liquid structure [10]. For example, neutron studies of multi-component silicate glasses [11–13] have advanced the understanding of how silicate frameworks are modified upon addition of minor components. One important advantage of using neutrons, as opposed to X-rays, is that the neutron scattering length is not directly proportional to atomic number but instead varies irregularly across the periodic table and even between isotopes of the same element. This fact can be exploited to produce scattering contrast using the technique of isotope substitution. Indeed, in some cases it is possible to mix isotopes in such a manner that there is no structural contribution to the diffraction pattern from a given element – the so-called 'null scattering' technique [13–15]. Thus, a first-order isotope difference of the diffraction patterns from a 'null scattering' sample and another, otherwise identical, sample differing in isotope enrichment, yields detailed and unambiguous information on the local environment around the substituted element. This method has been successfully used to examine the structural role of various elements such lithium, calcium, titanium and nickel [15,16], as well as RE elements such as Dy(III) [17], the latter being the focus of the present study.

In this paper, we present the results of a neutron diffraction study of lanthanide-bearing sodium silicate glasses. Isotopic substitution of dysprosium forms a central part of this study. The aim was to investigate the structural role of the RE ion as derived from the real-space pair correlation functions. The diffraction data are also used in combination with Reverse Monte Carlo modeling [18,19] to provide suggested structures for the RE-bearing glasses. These findings are later compared to those from earlier calorimetric and spectroscopic studies on glasses and liquids of similar composition.

2. Experimental methods and theory

The samples were all based on the same sodium trisilicate composition ($Na_2O \cdot 3SiO_2$) used in high temperature calorimetry experiments, in which the heats of solution of RE_2O_3 in this base liquid were measured [20,21]. Similar RE-bearing sodium silicate glasses have also been studied using Raman and NMR spectroscopy [22]. Four glasses were synthesized; a sodium trisilicate (Na3S) base glass, two dysprosium-bearing samples each containing 6 mol% Dy_2O_3, and a 6 mol% La_2O_3 sodium trisilicate glass. All the glasses were made from mixtures of previously dried SiO_2 and $Na_2O \cdot CO_2 \cdot H_2O$, and Dy_2O_3 or $La(OH)_3$ powders. Appropriate amounts of these starting materials were shaken in a plastic bottle in order to make a homogeneous mixture that was then decarbonated in a platinum crucible overnight at 1273 K in a muffle furnace before fusing at 1573 K in a Deltech platform furnace. Each sample was then was quenched in air, removed from the crucible, crushed, and fused again. The compositions and chemical homogeneity of the glasses were later verified by electron microprobe analysis (Table 1).

Two dysprosium-bearing sodium silicate glass samples were made, one containing dysprosium in natural abundance (^{nat}Dy), and the other a 'null scattering' mix of isotopes (^{null}Dy). Natural dysprosium consists of a mixture of seven isotopes and has a coherent bound scattering length of 16.9×10^{-15} m (Table 2). The 'null scattering' sample was prepared by mixing natural dysprosium with enriched ^{162}Dy, which has a scattering length of -1.40×10^{-15} m, in the ratio 1.4:16.9 (^{nat}Dy:^{62}Dy). Because ^{162}Dy has a negative scattering length, such a mixture results in a net zero coherent scattering contribution from dysprosium. The ^{162}Dy isotope used was obtained in the form of the oxide ($^{162}Dy_2O_3$) from Oak Ridge National Laboratory. The Dy-bearing sodium trisilicate glasses each had 6 mol% Dy_2O_3 added to the base composition, enough to determine the structural influence of Dy(III) on the silicate structure without causing saturation.

The neutron diffraction experiments were performed using the glass, liquids and amorphous materials diffractometer (GLAD) at the intense pulsed neutron source (IPNS), Argonne. All measurements were carried out at room temperature using vanadium sample containers mounted on an automatic sample changer. In addition to the samples, data were also collected for a vanadium rod standard, an empty sample can, and the instrument background. The neutron scattering results for the Dysprosium glasses were complicated by the presence of a high-energy absorption resonance due to the ^{164}Dy isotope. To avoid the effects of this resonance, data corresponding to high neutron energies were omitted when aggregating the counts

Table 1
Compositions (atom fractions) and number densities of silicate glass samples

Element	Na3S base glass	Base glass + 6 mol%		
		$^{nat}Dy_2O_3$	$^{null}Dy_2O_3$	La_2O_3
Na	0.167	0.151	0.151	0.151
Si	0.250	0.226	0.226	0.226
La	–	–	–	0.039
^{nat}Dy	–	0.038	0.003	–
^{162}Dy	–	–	0.035	–
O	0.583	0.585	0.585	0.585
Number density (atoms/Å^3)	0.074	0.074	0.074	0.072

Table 2
Coherent bound scattering lengths for elements in RE-bearing sodium silicate glasses

Element	$\bar{b}_{coh}$ (10^{-15} m)
Na	3.58
Si	4.149
O	5.803
^{nat}Dy	16.90
^{162}Dy	−1.4
La	8.24

from each detector bank and this restricts the upper limit of the scattering vector (Q) to a maximum of 20 Å^{-1}. As a consequence, the real-space resolution for the Dy-bearing samples is reduced compared to the other glasses.

The diffraction data were corrected for multiple scattering and absorption using standard data analysis procedures [23,24]. This yields the measured differential cross-section which is related to the desired Faber–Ziman average structure factor, $S(Q)$, by

$$\frac{d\sigma}{d\Omega} = \langle \bar{b} \rangle^2 [S(Q) - 1] + \langle \bar{b^2} \rangle \quad (1)$$

For a multi-component system, $S(Q)$ is the average of the partial structure factors, $S_{ab}(Q)$, for each pair of atom types a and b, all weighted for concentration c and coherent scattering length $\bar{b}$ such that

$$S(Q) = \frac{1}{\langle \bar{b} \rangle^2} \sum_{ab} c_a c_b \bar{b}_a \bar{b}_b S_{ab}(Q) \quad (2)$$

The real-space correlation function $g(r)$ is obtained from this quantity using the following Fourier transform relationship

$$g(r) = 1 + \frac{1}{2\pi^2 \rho_0} \int_0^\infty (S(Q) - 1) \frac{\sin Qr}{Qr} Q^2 \, dQ \quad (3)$$

where ρ_0 is the atomic number density of the sample. This quantity is also a composition and neutron-weighted average of partial pair functions, $g_{ab}(r)$, such that

$$g(r) = \frac{1}{\langle \bar{b} \rangle^2} \sum_{ab} c_a c_b \bar{b}_a \bar{b}_b g_{ab}(r) \quad (4)$$

For the purposes of modeling and interpreting our real-space data, we shall use the total correlation function, $T(r)$, which is defined as

$$T(r) = 4\pi \rho_0 r g(r) \quad (5)$$

$T(r)$ has the useful property that the broadening effects of instrument resolution and the finite upper data limit are symmetric and independent of radial distance r. Note that no corrections were made for paramagnetic scattering and consequently there are some clearly unphysical features at low r in the real-space data presented. Fortunately, these have no bearing on the features of interest at higher r.

The structure of the rare earth-bearing sodium silicate glasses can be evaluated by reverse Monte Carlo models. Reverse Monte Carlo modeling [18] uses a three-dimensional arrangement of atoms as a starting configuration. This may be based on a crystal structure or random distribution of atoms. The simulations used 3000 atoms fitted in reciprocal to the neutron data. $T(r)$ data was used to constrain the minimum approach distances between two atom types and coordination constraints were determined from the real space data for natural and isotopically substituted glasses. The Si–O coordination was maintained at 4.0 and the Si–O distances constrained to be between 1.4 and 1.8 Å. For Dy–O, the average coordination number and cut-off distances were also determined from the isotopically substituted real space data. Once an initial configuration is established atoms are moved randomly one at a time and the structure factor calculated and compared to experimental data. If the random move improves the agreement with the experimental data then the move is accepted with some probability. The random movement of atoms is continued until the difference between the modeled and experimental data is minimized. Reverse Monte Carlo has proven to be effective in analyzing glassy or amorphous materials particularly if independently derived constraints, coordination numbers form NMR, X-ray or EXAFS, are used. Although the simulation tends to give the most disordered structure consistent with the data, differences between the structures of glasses discussed in this paper are quite evident.

3. Results

Total structure factors for all the glass samples are shown in Fig. 1, and the Faber–Ziman weighting coefficients (arising from the constants in Eq. (2)) for each partial pair term are shown in Table 3. The first diffraction peak in the sodium silicate (Na3S) base composition is seen at 1.7 Å^{-1}, and this is also present in the RE-bearing glasses although the magnitude has decreased and the peak is broader, which suggests a change in network connectivity on addition of the RE ion [25]. There are also prominent peaks at ≈2.9 and 5.4 Å^{-1} in the base glass that decrease in magnitude in the Dy-bearing samples. In contrast, the structure factor for the La-bearing sample shows little change when compared to that of the base glass.

The corresponding real-space $T(r)$ functions are shown in Fig. 2. These have all been produced by Fourier transformation using a common upper data limit of $Q_{max} = 20$ Å^{-1}, thus allowing the data to be compared at the same real-space resolution. In the later, more detailed, discussions of each sample, we will make use of the full data range and hence real-space resolution available. The

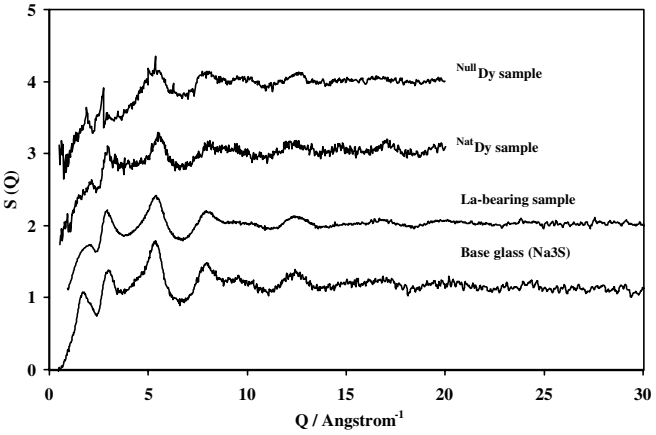

Fig. 1. Total structure factor measurements for sodium silicate-based glass samples. Other than for the base glass, the data have been successively offset vertically by +1 for clarity.

Table 3
Faber–Ziman coefficients for RE-bearing sodium silicate glasses

	Na3S	Na3S + 6 mol%		
		$^{nat}Dy_2O3$	$^{null}Dy_2O_3$	La_2O_3
O–O	0.4557	0.3775	0.485	0.4276
Si–O	0.2782	0.2091	0.2686	0.2368
Na–O	0.1601	0.1201	0.1544	0.1361
Na–Si	0.0491	0.0332	0.0426	0.0375
Si–Si	0.0428	0.0289	0.0371	0.0327
Na–Na	0.0139	0.0096	0.0123	0.0108
RE-O	–	0.1448	–	0.0799
RE-Si	–	0.04	–	0.0221
RE-Na	–	0.0230	–	0.0127
RE–RE	–	0.0139	–	0.0037

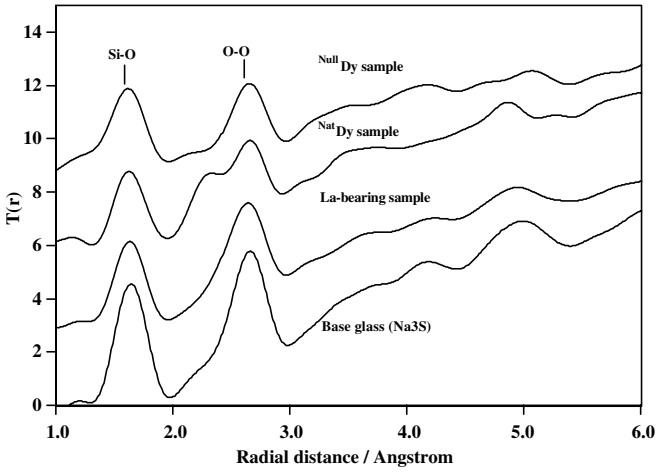

Fig. 2. Total pair correlation functions for all glass samples. The $T(r)$ data have been obtained by Fourier transformation of the corresponding $S(Q)$ data using the *same* value of Q_{max} (20 Å^{-1}). Again, other than for the base glass, the curves have been successively offset vertically for clarity.

first major peak in $T(r)$ is the Si–O bonding peak at approximately 1.64 Å. The next peak at about 2.65 Å is from the O–O non-bonding, nearest-neighbor correlation. These two peaks represent the local structure of the silicate tetrahedron, the main structural unit in these glasses. The Si–O peak is present at the same radial distance in all the glasses studied, and for the same Q_{max}, the width of this peak is identical. In the case of the sodium silicate base glass, there is a broad asymmetric peak centered at 2.33 Å appearing as a shoulder to the O–O correlation. In addition, there are distinct structural features out to distances of 6 Å, for example, the peaks at approximately 4.2 and 5 Å. These features reflect the range II and III order of Wright [11], i.e., the interconnectivity of the structural units and the network topology. The range II and III features cannot be interpreted in detail, however, without a structural model. Again, the $T(r)$ function for the La-bearing sample shows the least change compared the base glass. The most obvious difference is the superimposition of the La–O correlation on the low-r side of the O–O peak. This leads to a broadening of the resulting composite peak as well as a shift in the main peak to slightly lower r. Changes in the range II and III regions can also be seen. The ^{nat}Dy glass exhibits a prominent peak at 2.3 Å, which must be due to the nearest-neighbor Dy–O correlation since this feature is noticeably absent in the 'null scattering' sample. At higher r, there are further differences between the real-space functions for the two Dy-bearing glasses. For example, the broad feature at about 3.6 Å and the sharp peak at 4.8 Å are both less prominent in the 'null scattering' sample.

All four glasses are based on the same sodium silicate (Na3S) composition. This is a network-modified silicate, that is, a framework of corner shared SiO_4^{4-} tetrahedra modified by monovalent sodium ions. This means that the Si–O and O–O correlations are unlikely to be change in the $T(r)$s for all four glasses and can be eliminated from the $T(r)$s to identify changes in the correlations of the network-modifier (Na–O) and to distinguish the Dy–O and La–O correlations. Using the highest real-space resolution data available, we now proceed to discuss the results for each sample in more detail.

4. Sodium silicate base glass

The high-resolution $T(r)$ function ($Q_{max} = 30$ Å^{-1}) for the Na3S base glass is shown in Fig. 3. Information about individual coordination shells can be derived from $T(r)$ by fitting Gaussians convolved with a peak shape function to take into account the effects of the window function and finite Q_{max} used in the Fourier transform from $S(Q)$ [24]. Using this approach on the nearest-neighbor Si–O peak, a value of 3.98 was obtained for the average number of

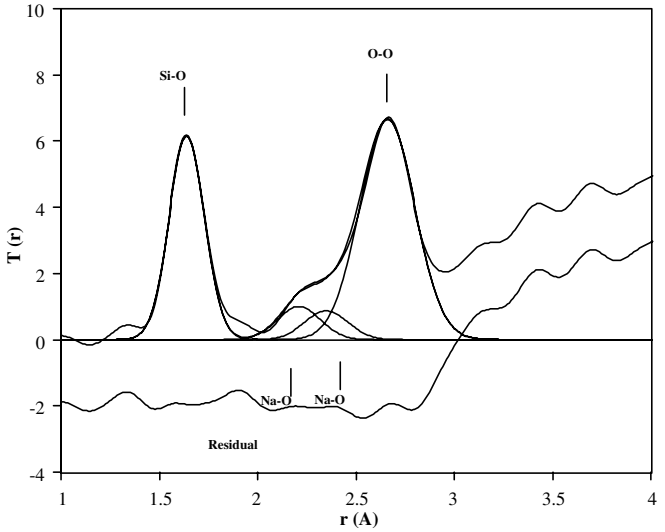

Fig. 3. Gaussian fits to $T(r)$ for sodium silicate base glass with Q_{max} of 30 Å^{-1}. The basic structural unit, the SiO_4^{4-} tetrahedron, is represented by two correlations; a Si–O distance at 1.64 Å, and a O–O distance at 2.65 Å. There are two Na–O correlations at 2.20 and 2.39 Å due to sodium ions coordinated by non-bridging and bridging oxygens, respectively.

oxygen atoms around silicon. This result is very close to the ideal value (4) expected for the SiO_4^{4-} tetrahedron and thus provides confirmation of the high quality of the data. The positions of the Si–O and O–O peaks also remain nearly identical to those in vitreous SiO_2. However, the broad asymmetric shoulder to the O–O peak seen earlier in Fig. 2 can now be clearly resolved into two separate peaks due to Na–O correlations. An earlier neutron diffraction study of Na3S glass by Clare et al. [26] was unable to resolve these features because data was only collected out to a Q_{max} of 22.5 $Å^{-1}$, compared to 30 $Å^{-1}$ for the present data. The existence of two distinct Na–O nearest-neighbor distances reflects the non-random distribution of sodium ions in alkali silicate glasses, a result expected in the modified random network model. Because of stochiometric considerations [27,28], negatively charged non-bridging oxygens (NBOs) will tend to cluster towards positively charged network-modifying cations such as Na^+. Bridging oxygens (BOs) provide the network connectivity between SiO_4^{4-} tetrahedra and the resulting constraints lead to a non-random distribution of the sodium-rich clusters. Such a non-random distribution of sodium ions will mean that although positive Na^+ ions will adopt an optimum configuration with respect to the negatively charged NBOs, their tendency to cluster means that not all the oxygen surrounding the sodium ions will be non-bridging. Thus, there will be two contributions to the Na–O correlation; from bridging and non-bridging distances. Distances of 2.21 and 2.35 Å corresponding to Na^+ correlations with NBOs and BOs, respectively, were obtained from a least-squares fit using two Gaussians (Table 4). Bond–valence theory [29] can be used to predict coordination numbers for the different types of oxygen atom around sodium. Using this approach, close to 5 bridging oxygens are expected around each Na^+ ion whereas the number of NBOs is around 3. These values are consistent with the percolation domain models for alkali silicate glasses [27,30] with alkali-rich regions within a polymerized silicate framework.

Table 4
Results of fitting Gaussian peaks to the $T(r)$ data

Sample	Constrained peaks			Fitted peaks			
	Peak	Midpoint	Sigma	Peak	Midpoint	Sigma	CN (calc)
Na3S							
	Si–O	1.64	0.09	Na–O	2.21	0.09	2.9
	O–O	2.67	0.12	Na–O	2.35	0.12	4.9
Na3S + ^{nat}Dy							
	Si–O	1.64	0.12	Dy–O	2.29	0.12	5.9
	O–O	2.67	0.16				
Na3S + ^{null}Dy							
	Si–O	1.64	0.14	Na–O	2.15	0.13	2.6
	O–O	2.67	0.16	Na–O	2.35	0.13	4.4
Na3S + La							
	Si–O	1.64	0.13	La–O	2.48	0.12	6.0
	O–O	2.67	0.17	Na–O	2.15	0.12	2.6
				Na–O	2.35	0.15	4.4

A model configurations or the Na3S base glass can be obtained by reverse Monte Carlo fit to the neutron diffraction data. A random silicate network is established with all silicon atoms coordinated by four oxygen atoms. The closest Si–O and Si–Si distances were obtained form literature values and confirmed by the diffraction data. An average Na–O coordination number of 4.9 was added as a constraint based on the apparent mixture of $Na–O_{BO}$ and $Na–O_{NBO}$ distances estimated from the pair correlation functions ($T(r)$) (Fig. 3). The results of this fitting procedure are showing in Fig. 4 as a fraction of the overall 3000 atom configuration. This model structure clearly shows the corner-shared SiO_4 network with Na-rich domains with Na^+ ions coordinated by both bridging and non-bridging oxygen. It is easy to visualize from this structure that Na^+ ions would be mobile in these percolation domains and would enhance ionic conductivity.

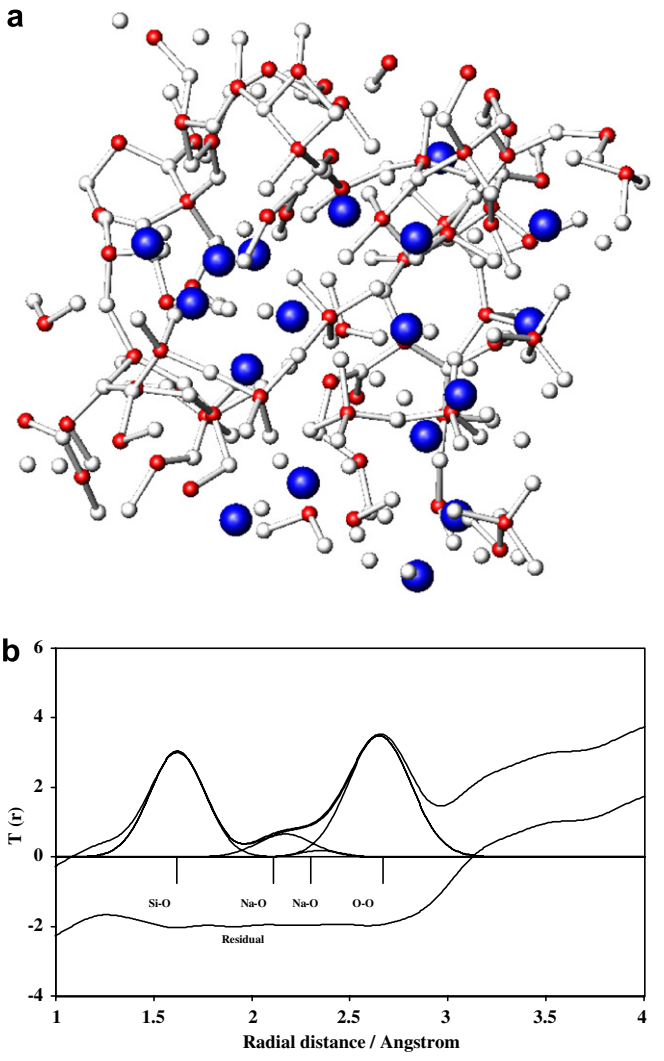

Fig. 4. Results of a reverse Monte Carlo fit to the diffraction data for Na3S glass. This portion of the 3000 atom configuration shows a network of corner shared silicate tetrahedral and sodium atoms heterogeneously distributed throughout the configuration in sodium-rich percolation domains.

5. Dy-bearing sodium silicate glass

The full resolution $T(r)$ functions for the dysprosium-bearing glasses ($Q_{max} = 20$ Å^{-1}) are shown in Fig. 4. The width of the Si–O peak (Fig. 5) is comparable to that of the base glass and the Si–O distance is identical. A Gaussian fit to this peak in $T(r)$ for the ^{nat}Dy sample yields a mean coordination number of 4.093. For the ^{Null}Dy sample, the corresponding coordination number is 3.905. These values indicate that there is virtually no change in the silicate tetrahedra themselves when dysprosium ions are added.

The most obvious difference between $T(r)$ for the ^{nat}Dy-bearing sample and the Na3S base glass is the presence of a peak corresponding to the nearest-neighbor Dy–O distance. The first-order isotope difference between the neutron diffraction data for the ^{nat}Dy- and ^{null}Dy-bearing glasses can be expressed in the Faber–Ziman formalism as:

$$\Delta S(Q) = 0.653 S_{Dy-O}(Q) + 0.180 S_{Dy-Si}(Q) + 0.104 S_{Dy-Na}(Q) + 0.063 S_{Dy-Dy}(Q) \quad (6)$$

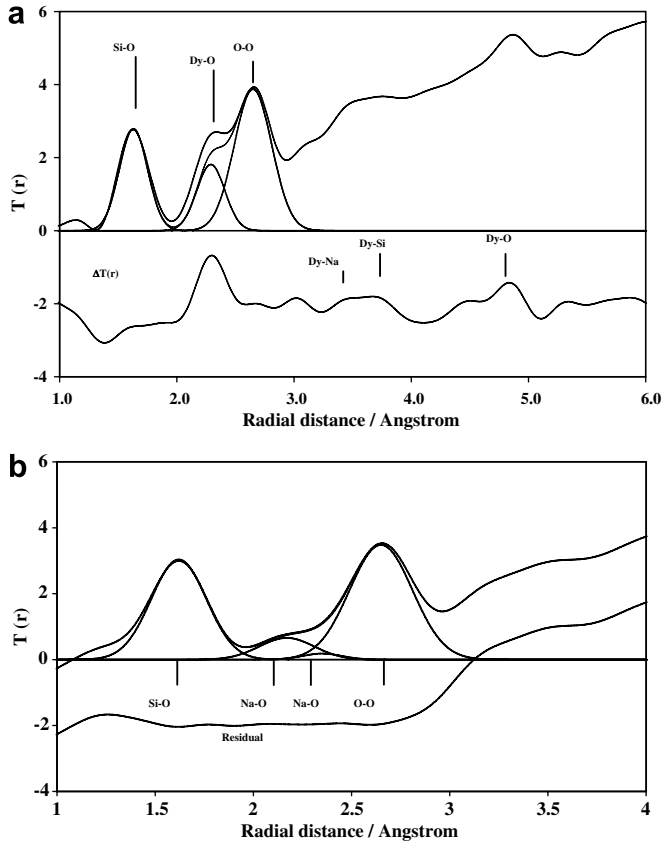

Fig. 5. (a) Gaussian fits to $T(r)$ for ^{nat}Dy glass. In addition to the Si–O and O–O distances, the Dy–O peak is fit at a distance of 2.3 Å. The parameters of the Dy–O peak have been obtained by fitting a Gaussian to the lower curve representing the difference in $T(r)$ between the ^{nat}Dy and ^{null}Dy samples ($\Delta T(r)$). (b) Gaussian fits to $T(r)$ for ^{null}Dy glass. The changes in the Na–O correlation, notably the increase in the magnitude of the Na–O peak at shorter distance associated with coordination by non-bridging oxygen, suggest disruption of the existing sodium silicate framework.

(NB the weighting coefficients of difference partial terms have been re-normalized to add up to unity). The real-space correlations involving dysprosium can thus be uniquely determined in the $\Delta T(r)$ function corresponding to this $\Delta S(Q)$. As can be seen from the lower part of Fig. 4a, the greatest contribution to $\Delta T(r)$ is from the Dy–O nearest-neighbor correlation at $r = 2.29$ Å. By fitting a Gaussian to this peak (Fig. 5), a mean coordination number of 5.9 oxygen atoms around each Dy(III) ion was obtained. Bond–valence theory can also be used to establish the coordination number based on the nearest-neighbor distance and confirms a Dy–O coordination number of about 6.0. Our distance for the Dy–O first peak is very similar to that obtained for Dy–F in a study of Dy-bearing BeF glass [26].

The isotope difference between the ^{Nat}Dy- and ^{null}Dy-bearing glasses can be used to further delimit the influence of Dy(III) ions on the silicate glass structure (Fig. 5). In particular, there are two broad features in $\Delta T(r)$ at about 3.6 and 4.85 Å. Based on a consideration of the weighting factors (see Eq. (6)) and inter-atomic distances, the broad peak at 3.6 Å is most likely a combination of peaks from Dy–Na and Dy–Si, with the latter correlation occurring at slightly greater radial distance than the former. The broad peak at 4.85 Å is most likely from Dy–O second distances simply because of its size (Dy–O clearly has the greatest weighting and dominates $\Delta T(r)$). This peak is asymmetric, which may indicate the formation of clusters of Dy–O octahedra (i.e., two sets of Dy–O second distances; one at 4.49 Å and one at 4.85 Å, reflecting clustered and non clustered DyO_6 units) although without a structure model the effects of clustering on the real-space distances cannot be determined unequivocally. The weighting of the Dy–Dy contribution to $\Delta T(r)$ is rather small for this oxide glass and hence cannot be readily assigned.

Because they no longer overlap, the absence of the Dy–O nearest-neighbor peak in $T(r)$ for ^{null}Dy allows us to gauge the effects of RE ions on the Na–O correlations (Fig. 5). As is apparent from Table 3, The ^{null}Dy real-space correlation function can be compared almost directly to that of the base glass (Fig. 3). There is a decrease in the magnitude of the broad Na–O correlation in the ^{null}Dy sample and this decrease is greater than that anticipated from the small difference in the Faber–Ziman weighting coefficients (Table 3). The Na–O peak at the shorter radial distance is increased in magnitude relative to that in the base glass and is also shifted to a value of 2.17 Å, suggesting a slight decrease in coordination number. This apparent effect is investigated further by a reverse Monte Calo (RMC) fit to the diffraction data with Dy–O and Dy–Dy distances constrained by the difference in the pair correlation function (T(r)) between null-scattering and natural Dy-bearing glasses. A lower value of the average coordination constraint for Na–O was used (4.6). Using these constraints the addition of Dy_2O_3 to the sodium silicate glass structure has two effects. First, Dy–O polyhedra are seen

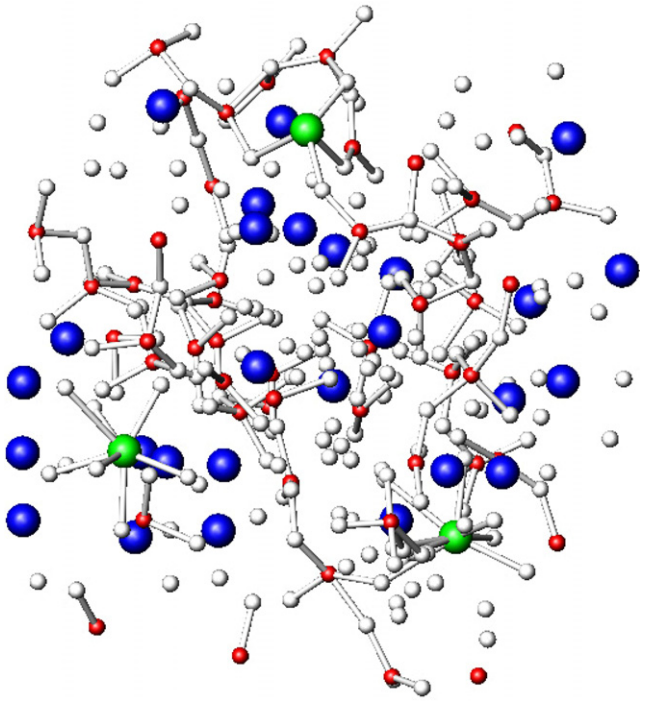

Fig. 6. Results of a reverse Monte Carlo fit to the diffraction data for Dy-bearing Na3S glass. This portion of the configuration shows that Dy(III) can form clusters that can link silicate units and act as a network former, disrupting the sodium rich percolation domains and also can form isolated, stable clusters within the sodium-rich domains. In some cases, the Dy–O polyhedra may be linked with shared (oxide-like) oxygen.

to form part of the silicate network with Si–O–Dy bridging bonds. Secondly, DyO_6 polyhedra form clusters within the Na-rich domains. In these latter configurations there is a suggestion that some of the oxygen remains 'oxide-like', i.e., there are Dy–O–Dy bonds and clusters of Dy–O polyhedra. This has been suggested for the La-bearing glasses by NMR and Raman spectroscopy [22], although there is no direct evidence for oxide-like oxygen in the neutron diffraction data and oxide-like oxygen is not used as a constraint in the RMC fitting procedure. A small portion of the 3000 atom configuration that was fitted to the neutron diffraction data is shown in Fig. 6.

6. La-bearing sodium silicate glass

NMR and Raman studies of La-bearing sodium silicate glasses indicate the presence of a specific, lanthanide Q^3 species made up of a La^{3+} ion associated, via a NBO, with a silicate tetrahedron [8,22,31] Results from calorimetry are consistent with the formation of an energetically stable cluster [20] and NMR data [22] suggests some non-silicate (oxide-like) oxygen may also be associated with the Ln^{3+} ion. The full-resolution $T(r)$ function ($Q_{max} = 30$ Å^{-1}) for our La-bearing glass sample is shown in Fig. 5. The data have been fit using several Gaussians (Table 4), with the large one for the O–O peak being constrained to the same distance as in the base glass. The La–O correlation appears as a shoulder to this O–O main peak and indicates a La–O distance of 2.48 Å. This distance corresponds to a first-neighbor coordination number of 6.0 for La–O from bond–valence Theory [29] and the La–O correlation can be resolved by fitting a Gaussian peak with coordination number 6.0 at the distance of 2.48 Å (Fig. 7).The Si–O, O–O and La–O correlations modeled in the $T(r)$ can be used to examine the change in Na–O environment as Lanthanum is added to the base composition by reverse Monte Carlo modeling. Using constraints similar to those used in the RMC fits to the Dy-bearing glass data a RMC configuration of the La-bearing glass (Fig. 8) shows, again, two responses to the presence of La(III); La–O bonds with silicate tetrahedra forming La–O units in the silicate network and isolated La–O clusted disrupting the sodium-rich percolation domains. These configurations are consistent with the formation of a 'lanthanide Q^3' species (Si–O–La) suggested form the NMR study and also the formation of linked La–O polyhedra by 'oxide-like' La–O–La. Again the la–O–La bonds are not specified in the constraints used in the RMC fit. This model structure is consistent with observed increases in the glass transition temperature [32] and more 'strong' viscosity behavior [32,33]. The changes within the Na–O environment suggest that the percolation domains within the sodium silicate liquids are disrupted by the presence of Ln(III) and that the formation of rigid, stable La-bearing structural units increases liquid viscosity. Heat of solution data [20] show an increased heat of solution of La_2O_3 in sodium silicate liquids when compared to potassium-bearing solvents, these calorimetric data are interpreted as a reflection of the competition between sodium and lanthanum ions for bridging oxygens. Compared to Na^+, the K^+ cation competes less effectively with lanthanum for the same bridging oxygens and this results

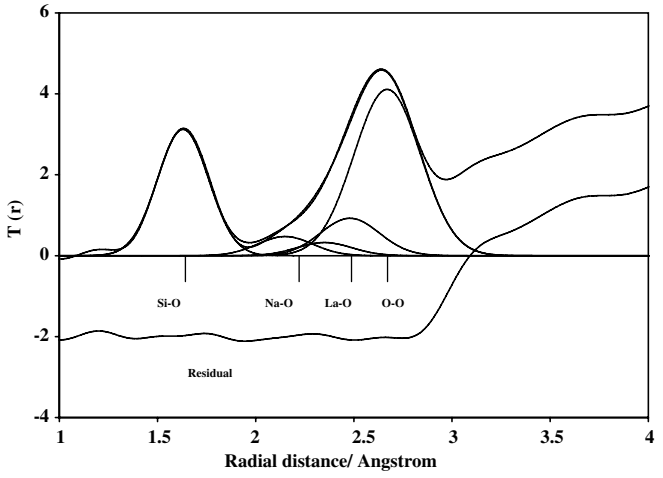

Fig. 7. Gaussian fits to $T(r)$ for La-bearing sodium silicate glass. The La–O correlation has been fit using a single Gaussian centered at a (La–O) radial distance of 2.48 Å. This is consistent with a first-neighbor coordination number for La(III) of 6.

in a more exothermic heat of solution for La_2O_3 [20] in potassium solvents.

The neutron diffraction data are in qualitative agreement with the results of a molecular dynamics simulation study of La-bearing sodium silicate glasses [34]. The La–O and O–O distances based on the molecular dynamics (MD) simulation are greater than those obtained from neutron diffraction and the La–O coordination number is also greater. The MD study indicates that the addition of lanthanide ions to the base sodium silicate composition modifies the network morphology, increasing the number of non-bridging oxygens. The non-bridging oxygens coordinate the lanthanum ion as suggested from the neutron diffraction data. In addition, the MD results show changes in the Na–Na distance, which is implied by the changes in Na–O correlations from the neutron diffraction data but is not determined directly. The MD simulations suggest that the La–O distance is greater in the sodium silicate glasses when compared to the lanthanum-bearing potassium silicate glasses, which have a reported La–O distance of 2.42 Å [34]. The neutron diffraction data show a La–O distance of 2.48 Å for the sodium silicate glasses. This suggests that the potential parameters used in the MD simulation underestimate the ability of the lanthanum ion to dictate its own coordination environment.

7. Correlation of the structural results with thermodynamic measurements

The heat of solution data for La_2O_3 in model alkali silicate liquids suggests a complex behavior of lanthanide ions in the molten state [20]. These calorimetric data show that the heat of solution of La_2O_3 is exothermic and the interaction between super-cooled La_2O_3 and the existing silicate framework is energetically favorable. The heats of mixing are small and are interpreted as reflecting formation of small, isolated, phase-ordered domains. This extreme form of clustering is supported by NMR and Raman spectroscopic measurements, which also suggest that there is isolation of oxygen from the silicate framework [22]. Recent molecular dynamics simulation of sodium silicate-based glasses with added La_2O_3[34] suggest that lanthanum ions adopt a network modifying role and result in formation of a non-bridging oxygen lanthanum bond ('lanthanide $Q^{3'}$) consistent with NMR and Raman data [2,8,22]. These simulation studies also confirm the presence of 'oxide' like oxygen which forms if La-polyhedra are linked by shared oxygen. The formation of these heterogeneities is consistent with the observed increases in viscosity as lanthanum is added to base alkali silicate compositions since the lanthanum-bearing units are rigid and will decrease self-diffusion, especially if the alkali-rich percolation domains are disrupted. The molecular dynamics simulations suggest only a small amount of non-silicate oxygen present – considerably less than suggested by the NMR and Raman data.

The diffraction data for the rare earth-bearing sodium silicate glasses confirm the formation of a six-coordinate lanthanide unit. Addition of the rare earth ion appears to disrupt the sodium-rich percolation domains, and depolymerize the existing silicate network through the formation of non-bridging oxygen leading to a decrease in overall network connectivity. The disruption of the sodium-rich domains is apparent as a decrease in the number of sodium ions coordinated by bridging oxygen and a corresponding increase in the coordination of sodium by non-bridging oxygen. This is most pronounced in the Dy-bearing glass since the two Na–O distances can be resolved unequivocally in the null-scattering Dy-bearing glass. The field strength of lanthanide ions (the ratio of formal change to ionic radius) increases as ionic radius decreases. Consequently, the Dy(III) ions would be expected to disrupt the existing silicate liquid the most when added. The heat of solution measurements for Dy_2O_3 in sodium trisilicate ($Na_2O{:}3SiO_2$) solvent is close to zero, this is more endothermic than for La_2O_3, although there are no differences in the $T(r)$ that would suggest a different solution mechanism. The differences in the heat of solution must reflect a greater interaction between the supercooled Dy_2O_3 and the transient silicate framework when compared to La_2O_3 as a result of the differences in ionic radius. This suggests a direct competition between sodium and lanthanide ions for the same bridging oxygen, consistent with the interpretation of the calorimetry data.

8. Conclusions

The local environment of lanthanide ions in sodium silicate glasses has been probed using the technique of neutron diffraction. Through the use of isotope substitution, the local structure around the dysprosium ion has been unambiguously determined, and the Dy–O nearest-neighbor peak position and coordination number obtained agree well with the predictions of bond–valence theory. The use of a 'null scattering' Dy isotope enrichment has also enabled the influence of the rare earth ion on the sodium structure to be discerned. The addition of dysprosium ions to the base sodium silicate glass appears to disrupt the alkali-rich percolation domains and results in the number of sodium ions coordinated by bridging oxygen. The structural mechanism for lanthanum appears identical to dysprosium with the only differences being due to the greater disruption of the silicate framework by the smaller ion (Dy^{3+}). Our structural data do not show any direct evidence for formation of non-silicate oxygen but are consistent with spectroscopy and thermodynamic data that favor formation of a specific lanthanide Q^3. The formation of such a lanthanide species would result in nanophase heterogeneities as suggested by spectroscopy. If the lanthanide polyhedra were clustered via corner-shared oxygen then this oxygen would be isolated from the silicate framework and be 'oxide-like' thus explaining the unusual influence of lanthanide ions on the behavior of silicate liquids.

Acknowledgements

This work has benefited from the use of the Intense Pulsed Neutron Source at Argonne National Laboratory. This facility is funded by the US Department of Energy, BES-Materials Science, under Contract W-31-109-Eng-38.

References

[1] M.R. Antonio, L. Soderholm, A.J.G. Ellison, J. Alloys Compd. 250 (1–2) (1997) 536;
H. Li, L. Li, J.D. Vienna, et al., J. Non-Cryst. Solids 278 (1–3) (2000) 35.
[2] A.J.G. Ellison, C.K. Loong, J. Wagner, J. Appl. Phys. 75 (10) (1994) 6825.
[3] Werner Lutze, Rodney C. Ewing, Radioactive Waste Forms for the Future, Elsevier Science Pub. Co., Amsterdam; New York, New York, NY, USA, 1988 (North-Holland; Sole distributors for the USA and Canada).
[4] B.T. Stone, K.L. Bray, J. Non-Cryst. Solids 197 (2–3) (1996) 136;
H. Takebe, K. Morinaga, T. Izumitani, J. Non-Cryst. Solids 178 (1994) 58.
[5] O. Menard, T. Advocat, J.P. Ambrosi, et al., Appl. Geochem. 13 (1) (1998) 105.
[6] Peter W. Lipman, Geological Survey (US), Rare-Earth-Element Compositions of Cenozoic Volcanic Rocks in the Southern Rocky Mountains and Adjacent Areas, Dept. of the Interior USG.P.O., Washington, DC, 1987.
[7] E.P. Vicenzi, T.H. Green, S.H. Sie, Nucl. Instrum. Meth. B 104 (1–4) (1995) 470.
[8] A.J.G. Ellison, P.C. Hess, J. Geophys. Res.-Solid Earth Planets 95 (B10) (1990) 15717.
[9] E.M. Larson, A.J.G. Ellison, F.W. Lytle, et al., J. Non-Cryst. Solids 130 (3) (1991) 260.
[10] G.E. Bacon, Applications of Neutron Diffraction in Chemistry, Pergamon Press, Oxford, New York, 1963 (distributed in the Western Hemisphere by Macmillan);
G.E. Bacon, X-ray and neutron diffraction, 1st ed., Pergamon Press, Oxford, New York, 1966;
G.E. Bacon, Neutron diffraction, 3d ed., Clarendon Press, Oxford [Eng.], 1975;
G.E. Bacon and International Union of Crystallography, Fifty years of neutron diffraction: the advent of neutron scattering. (A. Hilger, published with the assistance of the International Union of Crystallography, Bristol, 1986);
A.C. Barnes, M.A. Hamilton, P. Buchanan, et al., J. Non-Cryst. Solids 252 (1999) 393;
H.E. Fischer, P.S. Salmon, A.C. Barnes, Journal De Physique Iv 103 (2003) 359;
D.L. Price, J. Non-Cryst. Solids 76 (1) (1985) R7;
F.R. Trouw, D.L. Price, Ann. Rev. Phys. Chem. 50 (1999) 571.
[11] A.C. Wright, G.A.N. Connell, J.W. Allen, J. Non-Cryst. Solids 42 (1–3) (1980) 69.
[12] A.C. Wright, J. Non-Cryst. Solids 76 (1) (1985) 187;
D. Holland, A. Mekki, I.A. Gee, et al., J. Non-Cryst. Solids 253 (1999) 192;
P.H. Gaskell, M.C. Eckersley, A.C. Barnes, et al., Nature 350 (6320) (1991) 675.
[13] L. Cormier, P.H. Gaskell, G. Calas, et al., Phys. Rev. B 58 (17) (1998) 11322.
[14] L. Cormier, P.H. Gaskell, G. Calas, et al., Physica B 234 (1997) 393.
[15] L. Cormier, G. Calas, P.H. Gaskell, Chem. Geol. 174 (1–3) (2001) 349.
[16] C.A. Yarker, P.A.V. Johnson, A.C. Wright, et al., J. Non-Cryst. Solids 79 (1–2) (1986) 117;
J.H. Lee, A. Pradel, G. Taillades, et al., Phys. Rev. B 56 (17) (1997) 10934.
[17] A.G. Clare, G. Etherington, A.C. Wright, et al., J. Chem. Phys. 91 (10) (1989) 6380;
A.G. Clare, A.C. Wright, Rare Elements in Glasses 94 (9) (1994) 141.
[18] R.L. McGreevy, J. Phys. Condens. Matter 13 (46) (2001) R877;
R.L. McGreevy, Journal De Physique Iv 111 (2003) 347.
[19] R.L. McGreevy, P. Zetterstrom, J. Non-Cryst. Solids 293 (2001) 297.
[20] M.C. Wilding, A. Navrotsky, J. Non-Cryst. Solids 265 (3) (2000) 238.
[21] A. Navrotsky, Phys. Chem. Miner. 24 (3) (1997) 222.
[22] T. Schaller, J.F. Stebbins, M.C. Wilding, J. Non-Cryst. Solids 243 (2–3) (1999) 146.
[23] A.K. Soper, in: D.K. Hyer (Ed.), Advanced neutron sources, 1988: proceedings of the 10th Meeting of the International Collaboration on Advanced Neutron Sources (ICANS X) held at Los Alamos, 3–7 October 1988, Vol. 97, Institute of Physics, Bristol, England, New York, 1989, p. 890p.
[24] S. Susman, K.J. Volin, D.G. Montague, et al., J. Non-Cryst. Solids 125 (1–2) (1990) 168.
[25] J.H. Lee, S.R. Elliott, J. Non-Cryst. Solids 193 (1995) 133.
[26] A.G. Clare, A.C. Wright, R.N. Sinclair, J. Non-Cryst. Solids 213 (1997) 321.
[27] G.N. Greaves, Solid State Ionics 105 (1–4) (1998) 243;
G.N. Greaves, A. Fontaine, P. Lagarde, et al., Nature 293 (5834) (1981) 611;
G.N. Greaves, W. Smith, E. Giulotto, et al., J. Non-Cryst. Solids 222 (1997) 13;
W. Smith, G.N. Greaves, M.J. Gillan, J. Chem. Phys. 103 (8) (1995) 3091.
[28] W. Smith, G.N. Greaves, M.J. Gillan, J. Non-Cryst. Solids 193 (1995) 267;
N.M. Vedishcheva, B.A. Shakhmatkin, M.M. Shultz, et al., J. Non-Cryst. Solids 193 (1995) 292.
[29] N.E. Brese, M. Okeeffe, Acta Crystallogr. Sect. B-Struct. Sci. 47 (1991) 192.
[30] G.N. Greaves, J. Non-Cryst. Solids 71 (1–3) (1985) 203;
G.N. Greaves, Mineral. Mag. 64 (3) (2000) 441;
G.N. Greaves, K.L. Ngai, J. Non-Cryst. Solids 172 (1994) 1378.
[31] D.M. Krol, B.M.J. Smets, Phys. Chem. Glasses 25 (5) (1984) 119.
[32] J. Coon, J.E. Shelby, Phys. Chem. Glasses 35 (2) (1994) 47.
[33] J.T. Kohli, J.E. Shelby, Phys. Chem. Glasses 32 (2) (1991) 67.
[34] B. Park, L.R. Corrales, J. Non-Cryst. Solids 311 (2) (2002) 107.